

Computational Analysis Of Aerodynamic Characteristics With Different Overlap Ratio Using CFD

Dr.M.S.Murthy¹ & Ravishankar Kumrawat²

¹Director, Malwa Institute of Science & Technology (MIST), Indore M.P.-453111

²PG Scholar, Malwa Institute of Science & Technology (MIST), Indore M.P.-453111

Corresponding Author: Dr.M.S.Murthy

Abstract: Numerical investigation was carried out to find out aerodynamic characteristics with help of commercial computational fluid dynamic (CFD) software GAMBIT and FLUENT. In this analysis three different models with different overlap ratio were designed and fabricated for the current study to find the effect of overlap ratios. The results from the experimental part of the research show a significant effect of overlap ratio and Reynolds number on the improvement of aerodynamic performance of the Savonius wind turbine. At higher Reynolds number turbine Model without overlap ratio gives better aerodynamic coefficients and at lower Reynolds number Model with moderate overlap ratio gives better results.

Keywords:- FLUENT, overlap ratios, Reynolds number, aerodynamic coefficients

Date of Submission: 13-09-2018

Date of acceptance: 28-09-2018

I. INTRODUCTION

The two primary types of wind turbine are the horizontal axis wind turbine (HAWT) and vertical axis wind turbine (VAWT). HAWTs include both upwind and downwind configurations, with various performance enhancers, such as diffusers and concentrators. HAWTs are the most popular configuration now because they have higher efficiency, but they are only suitable for places with extremely strong, gusty winds and urban areas. Their technical development lags significantly behind that of HAWTs. However, HAWTs have never been proven fundamentally more aerodynamically efficient than VAWTs. Indeed, VAWTs may be more appropriate than HAWTs on a very large scale (10MW+) when the alternating gravitational loading on a HAWT blade becomes excessive. VAWTs have a number of advantages over HAWTs. First, they do not have to constantly yaw into the local wind direction. Second, due to their relatively lower rotational speed, they are typically quieter. Third, the cost of manufacturing very large VAWTs could be lower due to their simple, straight, constant section blades as compared to the HAWTs' complex, three-dimensional blades and, for the same reason, they could be easier to manufacture. Finally, VAWTs are mechanically better able to withstand high winds because their stalling behavior changes, offering a potential safety advantage during gust conditions. VAWTs include both a drag-type configuration, such as the Savonius rotor, and a lift-type configuration, such as the Darrieus rotor. Although the starting torque for Savonius rotors is high, it is not uniform at all rotor angles. The torque characteristics of an ordinary Savonius rotor have two problems. First, they vary significantly at different rotor angles, causing the rotor to vibrate and consequently decrease its durability. Second, the torque at the rotor angle ranging from 135° to 165° and from 315° to 345° is negative or very small, which hinders its use as a starter [11]. To decrease this torque variation and improve starting characteristics, a new type of Savonius rotor was designed and fabricated by Hayshi et al. [12]. It had three stages, with a 120° bucket phase shift between adjacent stages. With this design, wind-tunnel tests showed that both static and dynamic torque variations in one revolution were much smoother compared to an ordinary one-stage rotor, which greatly improved the starting characteristics. They also measured the torque characteristics of the rotors with guide vanes and found that, on the average the guide vanes increased the torque coefficient in the low tip-speed ratio but decreased it in the high tip-speed ratio. They concluded that two- and three-stage conventional Savonius rotors could overcome the problem of negative torque. However, the maximum power coefficient decreases for this kind of design with more stages.

To decrease the variation of static torque in conventional Savonius rotors with rotor angle ranging from 0° to 360°, Kamoji and Kedare [15] tested a helical rotor with a twist of 90°. They conducted experiments in an open-jet wind tunnel at gap ratios of 0.0, 0.05, and 0.08 to study the

effect of the overlap ratio and the Reynolds numbers on its performance to evaluate the static torque, the dynamic torque, and the power coefficients. They compared its performance with and without a shaft between the end plates at different overlap ratios. A helical rotor without a shaft was also compared with the

performance of the conventional Savonius rotor. They found that all helical rotors have a positive power coefficient of static torque for all rotor angles, but the rotors with a shaft had a lower power coefficient than those without. The power coefficient of the rotor without a shaft with a zero overlap ratio was marginally less than the conventional Savonius rotor. The rotor appeared to be sensitive to the Reynolds number, but this finding must be confirmed by rigorous experiments.

McWilliam and Johnson [18] investigated various Savonius wind turbine models to observe the vortex formation and the effect of the scale of downstream wake using particle image velocimetry (PIV) in a close loop wind tunnel. In that experiment, they used standard Savonius design (diameter = 30.18 mm) with two semicircular blades overlapping. The design of these blades include deep blade design (diameter = 31.20 mm), shallow blade design (diameter = mm), outside J blade design (diameter = 32.97 mm) and inside J blade design (diameter = 31.18 mm). They executed the experiment at a constant 3 m/s wind velocity. They observed that vortex shedding from the following blade was common to all five designs they tested, which had an effect on the scale of the downstream wake of the rotor. They found that the forward curved blade was the critical area for external flow and the overlap ratio of Savonius wind turbine blades allows flow from the top blade to enter the bottom blade that reduces the negative pressure region behind the blades.

Saha et al. [30] fabricated a two-stage Savonius wind turbine by inserting valves on the concave side of the blades. They compared its performance with a conventional Savonius wind

turbine and found that with valves on a three-bladed turbine, the power coefficient was higher compared to a two-bladed turbine for both semi-circular and twisted blades. Without valves, air strikes the blades and rotates them in a negative direction. They also varied the number of stages in a Savonius wind turbine and found that the power coefficient increase from a one-stage design to a two-stage design but decrease from a two-stage design to a three-stage design due to increased inertia. They tested twisted blades of one, two, and three-stages and found that three- stage design had a better power coefficient and the twisted-blade design showed better performance.

Three Bladed Savonius rotor Models

To observe the effect of overlap ratio (ratio between the distance of the two adjacent blades and rotor diameter) and Reynolds number on the aerodynamic characteristics of the Savonius rotor, three different rotor models with and without overlap ratio were designed and physically fabricated. These three models were tested in front of the subsonic wind tunnel for various Reynolds number flow conditions.

Savonius Rotor Model 1

The three bladed Savonius rotor model called Model 1 with no overlap between adjacent blades was designed and fabricated. Top, front, 3D design views and the fabricated scale model of the Savonius wind turbine are shown in Figure 3.4 (a), 3.4(b), 3.4(c) respectively. The model was made of three semi-cylindrical blades of diameter, $d = 127$ mm, and height, $H = 300$ mm. The turbine model was made of acrylic. The central shaft was removed from the turbine model. The blades were 120° apart from each other and the overall rotor diameter was $D = 248$ mm for the Model 1.

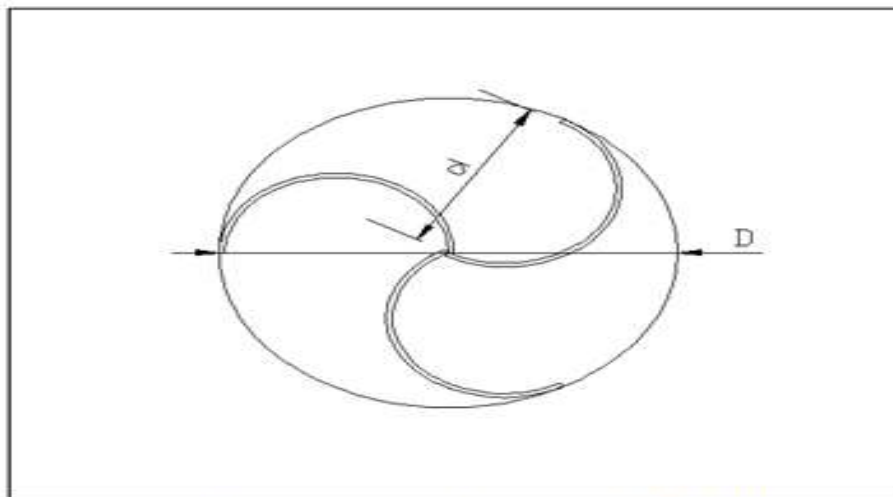


Figure 3.4(a): Top view of Model 1

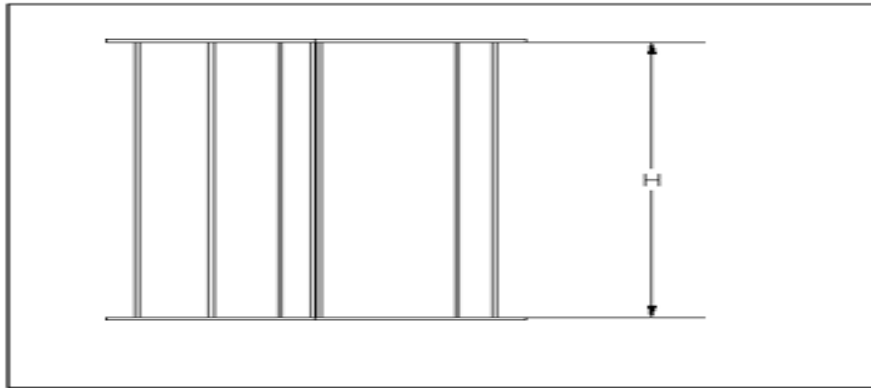


Figure 3.4(b): Front view of Model 1

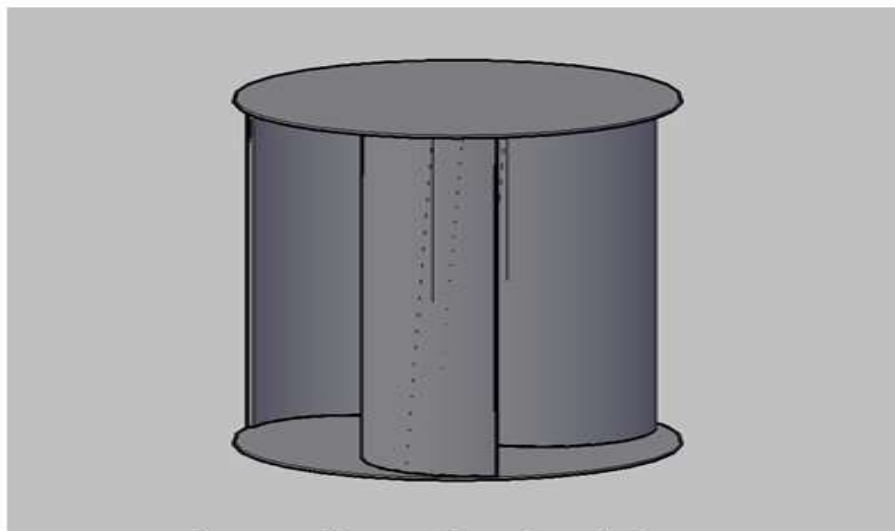


Figure 3.4(c): 3D view of Model 1

II. Numerical Procedure

The k- ϵ turbulence model was used for the computational flow simulation around the Savonius rotor models with different overlap ratios. Commercially available software FLUENT was used to solve the turbulent flow field and GAMBIT was used for mesh generation around the rotor models. Numerical simulation provides the pressure and velocity values at all nodal points of flow domain around the rotating blades. The purpose of this analysis was to observe the performance of various Savonius VAWTs configurations; it was felt that a 2-D simulation was sufficient for this application. Figures 3.15, 3.16, 3.17 show 2-D mesh generated within a computational domain around three bladed Savonius wind turbine models using GAMBIT in which the position of the three blades were 0° , 120° and 240° . The size of the computational domain was $1.6 \text{ m} \times 1.4 \text{ m}$ and the total number of nodes was around 39992. A size function was introduced with the rotor blade to get the better computational results adjacent to the blade surface. To introduce this size function the minimum mesh size near the blade surface was chosen $0.0005 \text{ m} \times 0.0005 \text{ m}$ with the growth rate of 1.1 and maximum mesh size was $0.008 \text{ m} \times 0.008 \text{ m}$. In this study triangular mesh was chosen over quadrilateral mesh to reduce the computational time. These generated meshes were then exported in FLUENT for post processing. The flow of air within the domain around the rotor model was assumed to be turbulent and the effects of molecular viscosity were considered negligible. The simplest "complete models" of turbulence are two-equation models in which the solution of two separate transport equations allows the turbulent velocity and length scales to be independently determined.

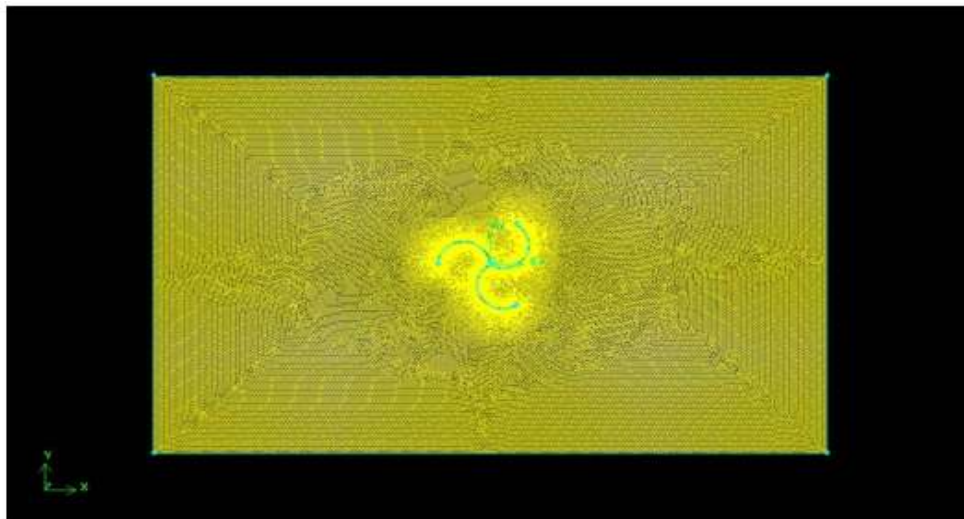


Figure 3.15: Generated mesh using Gambit for Model 1.

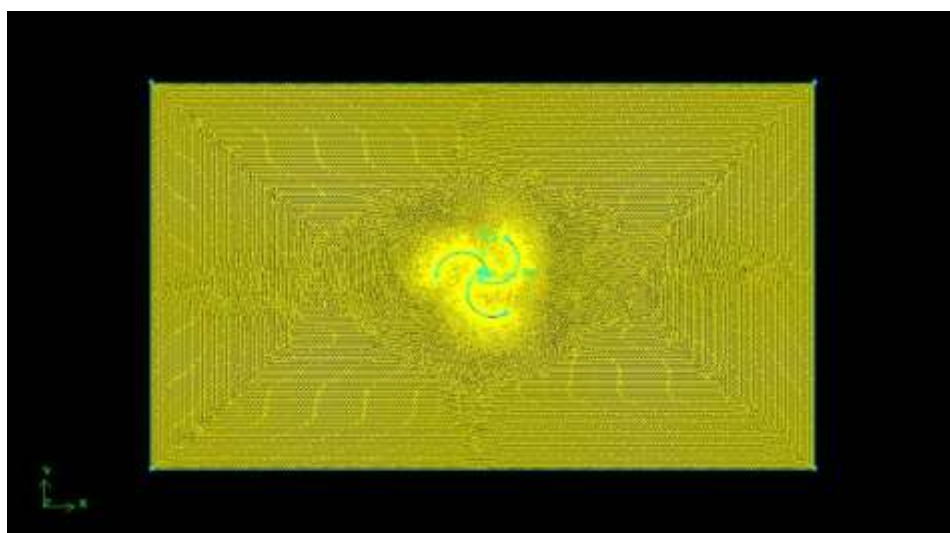


Figure 3.16: Generated mesh using Gambit for Model 2.

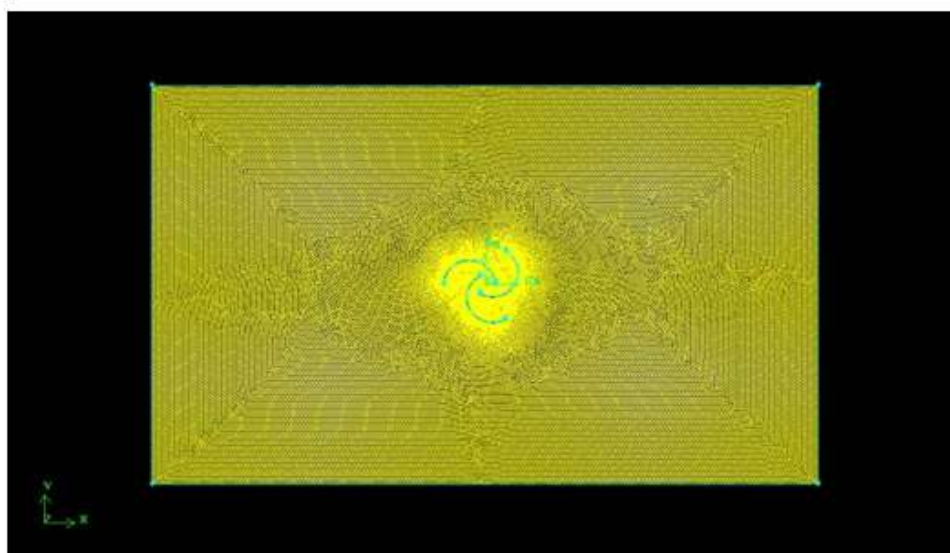


Figure 3.17: Generated mesh using Gambit for Model 3.

The standard k-ε turbulence model in FLUENT was used for the analysis of turbulent flow around rotor models. The pressure-velocity coupling is achieved using the well-known SIMPLE (Semi-Implicit Method for Pressure-Linked Equations) method by Patankar [22].

m/s, air density was considered 1.2 kg/m³. The blades were considered as moving walls and their rotational velocity was provided from the rpm measured during the experiment. The convergence of the sequential iterative solution is achieved when the sum of the absolute differences of the solution variables between two successive iterations falls below a pre-specified small number, which was chosen as 1×10⁻⁵ in this study. For all Models using k-ε turbulence model convergence criteria(1×10⁻⁵) was set and tested for continuity, x-velocity, y-velocity, kinetic energy (k) and turbulent dissipation rate (ε). It was found that for Model 1 at wind speed 9.66 m/s solution converged at 4019 iterations shown in Figure 3.18. For Model 2 and Model 3 at the wind speed 9.66 m/s solution converged respectively at 1844 and 1307 iterations.

III. Numerical Results

Pressure Contours for Three Models at Three Different Reynolds Number

Pressure contours generated from numerical simulation of **Model 1** for three different Reynolds number are shown in Figures 4.16 to 4.18. For all these cases higher pressure values were found at the convex side of the first blade Savonius rotor model. Negative pressure region was developed from convex side of blade 2 to some portion of convex side of blade 3. This negative pressure is creating pressure difference between concave and convex surface that eventually rotates the turbine blades.

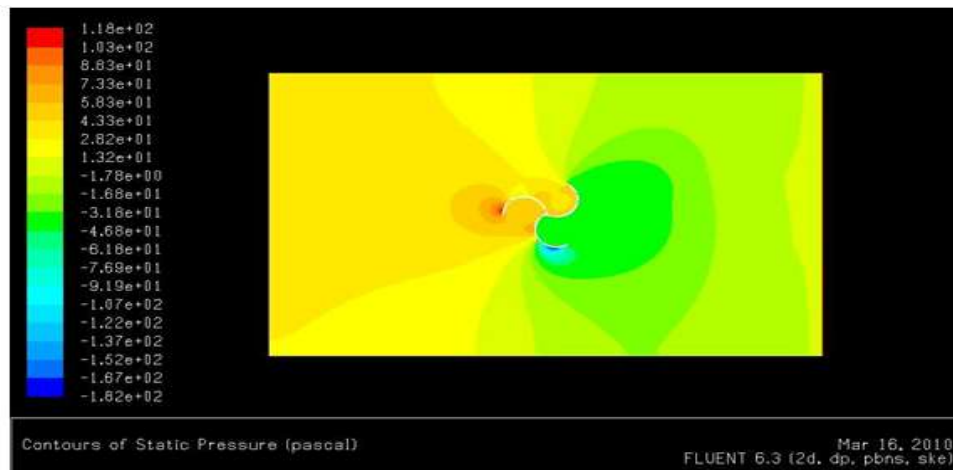


Figure 4.16: Pressure Contour around Savonius rotor Model 1 at $Re = 1.61 \times 10^5$.

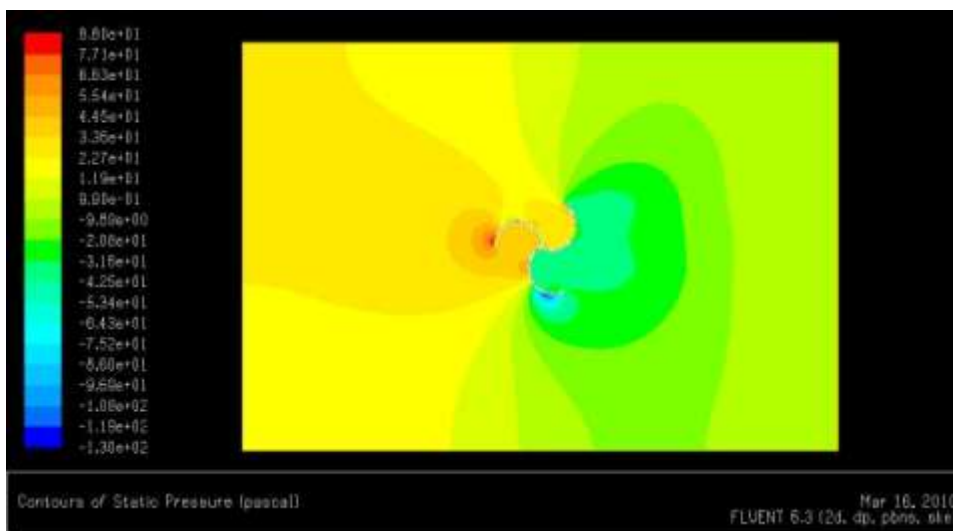


Figure 4.17: Pressure Contours around Savonius rotor Model 1 at $Re = 1.37 \times 10^5$.

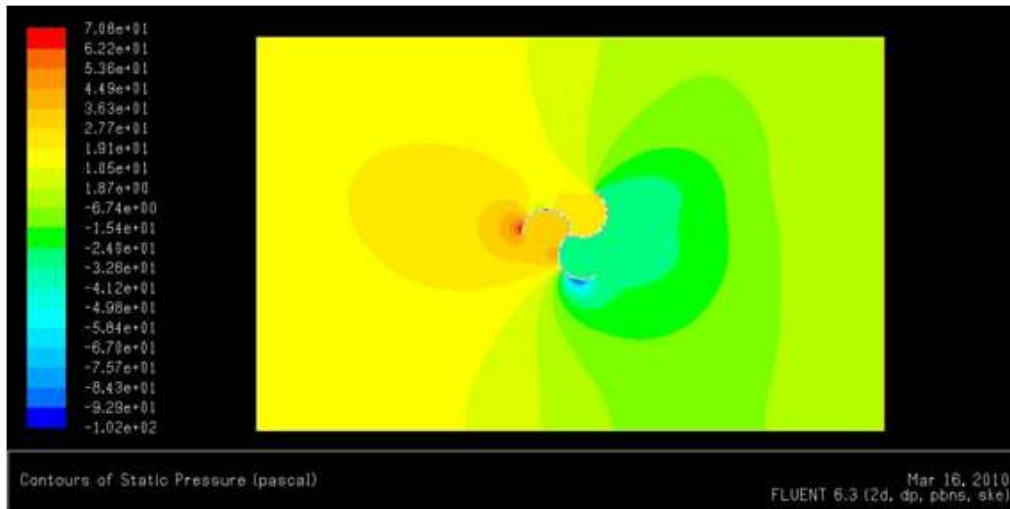


Figure 4.18: Pressure Contour around Savonius rotor Model 1 at $Re = 1.22 \times 10^5$.

Pressure contours around the Savonius rotor **Model 2** at three different Reynolds number are shown in Figures 4.19 to 4.21. Likewise Model 1 pressure contours the higher pressure region was developed at convex side of blade 1 and most negative pressure region was developed at outside of convex side of blade 3. Pressure contours around the Savonius rotor

Model 3 are shown in Figures 4.22 to 4.24.

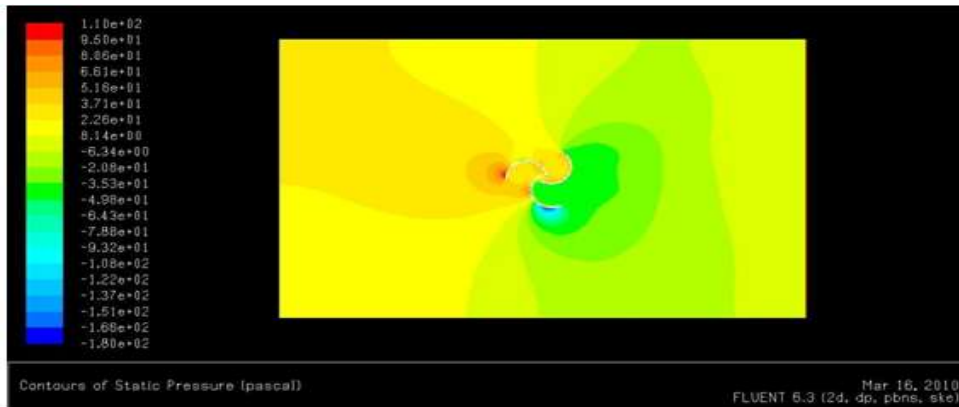


Figure 4.19: Pressure Contour around Savonius rotor Model 2 at $Re = 1.40 \times 10^5$.

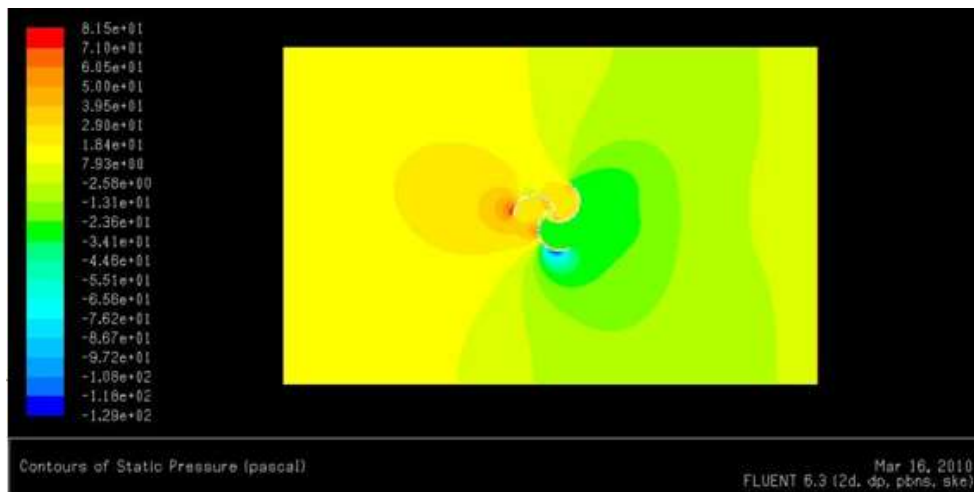


Figure 4.20: Pressure Contour around Savonius rotor Model 2 at $Re = 1.19 \times 10^5$.

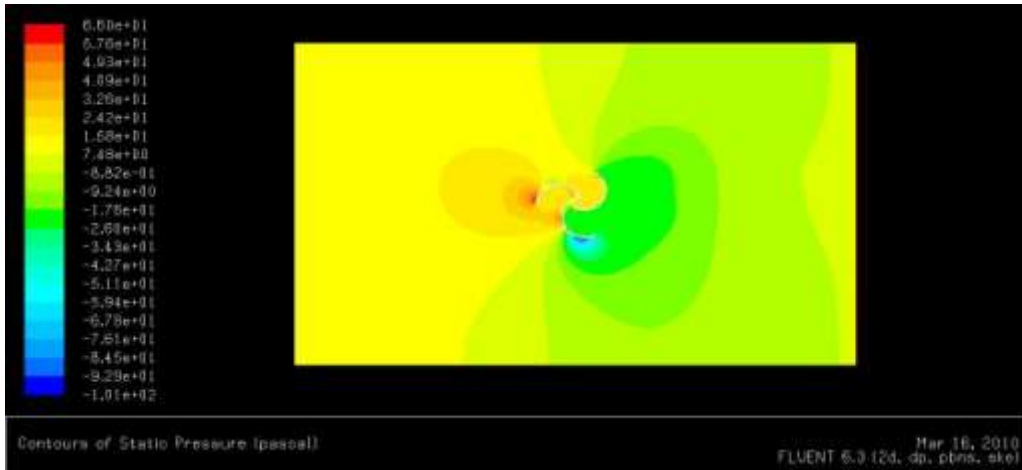


Figure 4.21: Pressure Contour around Savonius rotor Model 2 at $Re = 1.06 \times 10^5$.

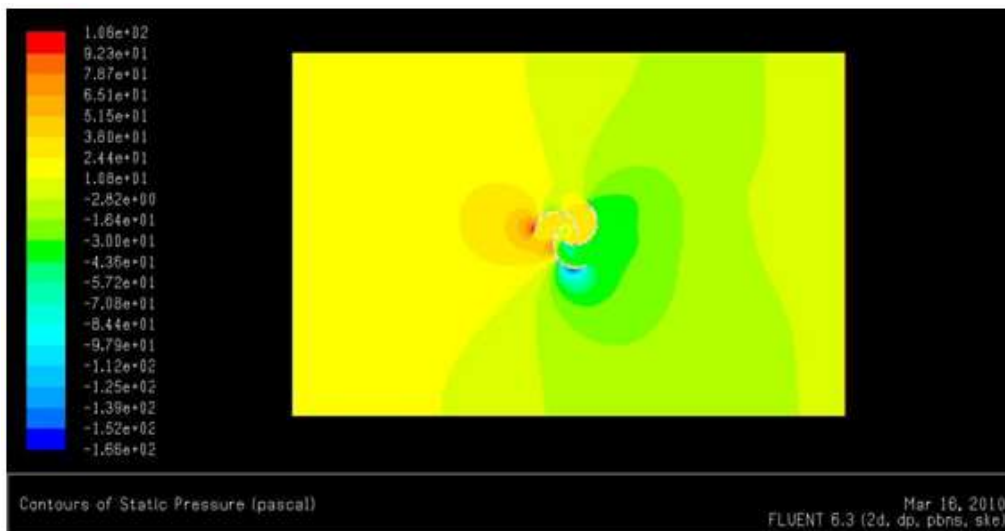


Figure 4.22: Pressure Contour around Savonius rotor Model 3 at $Re = 1.24 \times 10^5$.

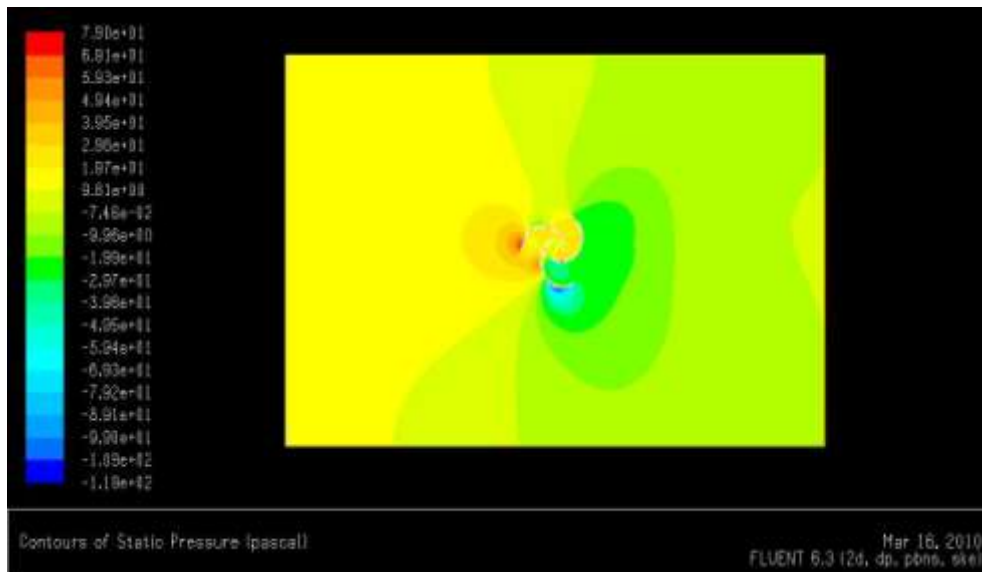


Figure 4.23: Pressure Contour around Savonius rotor Model 3 at $Re = 1.06 \times 10^5$.

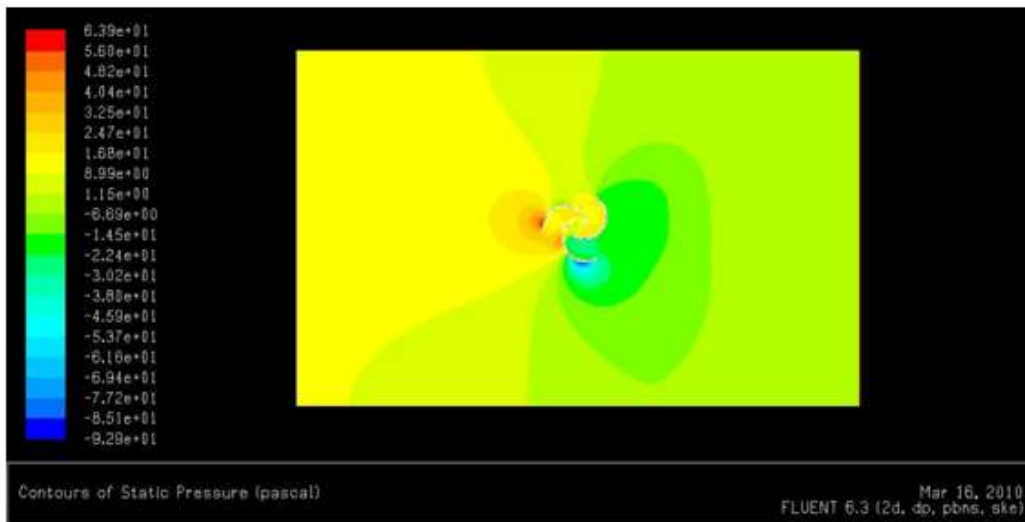


Figure 4.24: Pressure Contour around Savonius rotor Model 3 at $Re = 9.44 \times 10^4$.

Velocity Contours for Three Models at Three Different Reynolds Number

Contours of Velocity magnitude for Savonius rotor **Model 1** at three different Reynolds number are shown in Figures 4.25 to 4.27. Patterns of the contours are almost same for different Reynolds number only exception is a slight variation in velocity magnitude. Once the wind strikes the turbine blades the velocity starts to decrease at the trailing edge of the Savonius wind turbine model but after some distance travel starts to regain the velocity. Higher velocity region was created at the top and bottom side of the wind turbine model. Figures 4.28 to 4.30 show velocity contours for **Model 2** and Figures 4.31 to 4.33 show velocity contours for **Model 3** at different Reynolds number. Similar patterns of velocity contours are observed for Model 2 and Model 3 but only the velocity magnitudes are different for different model cases. From these figures it can be seen that with the increase of overlap ratio the lower velocity region shorten after the trailing edge and come closer to the turbine blades.

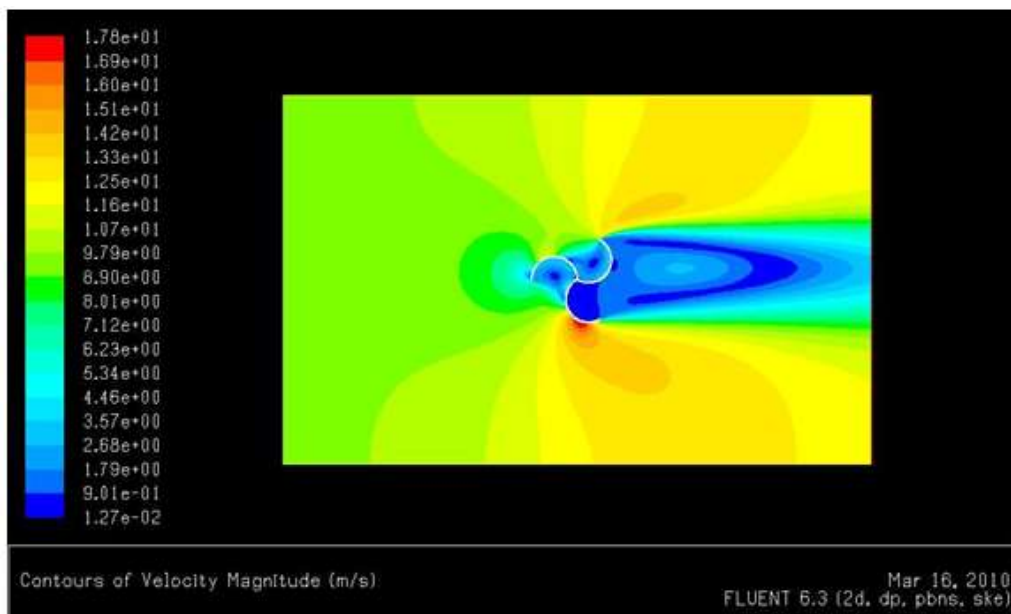


Figure 4.25: Velocity Contour around Savonius rotor Model 1 at $Re = 1.61 \times 10^5$.

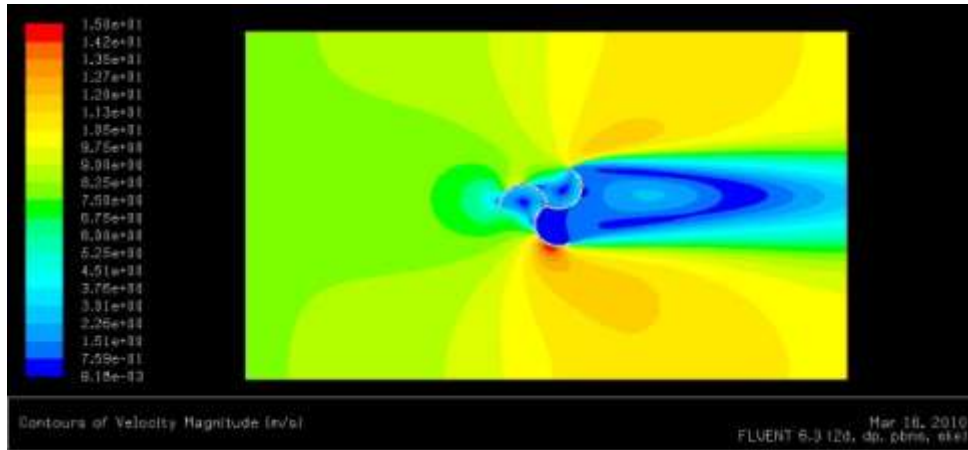


Figure 4.26: Velocity Contour around Savonius rotor Model 1 at $Re = 1.37 \times 10^5$.

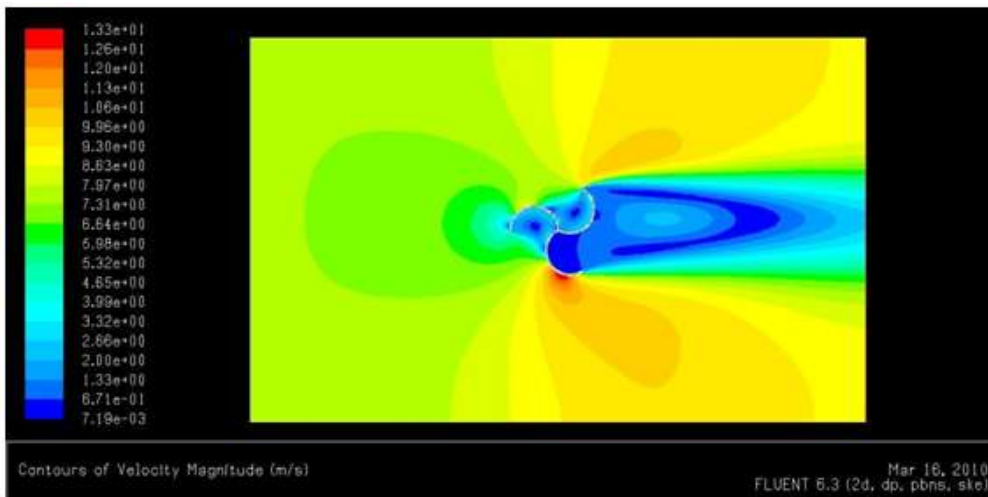


Figure 4.27: Velocity Contour around Savonius rotor Model 1 at $Re = 1.22 \times 10^5$.

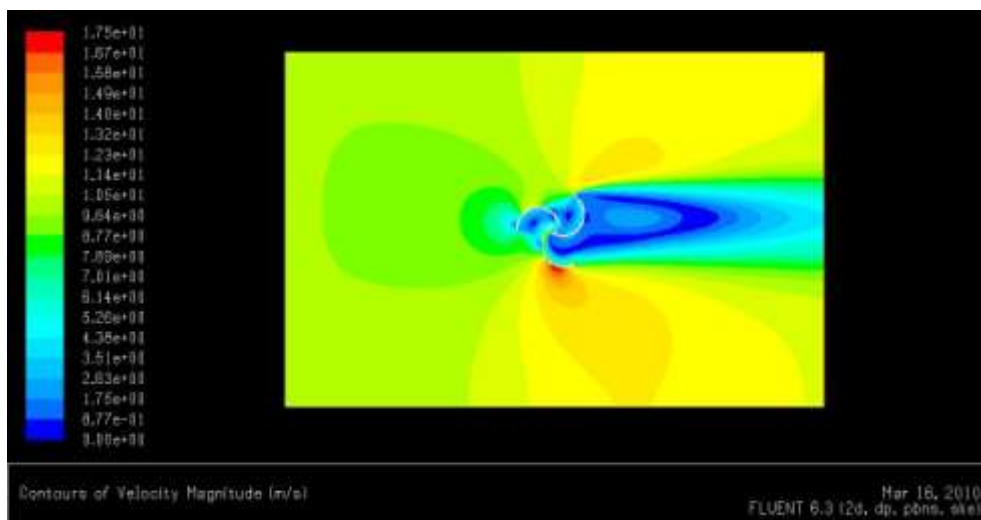


Figure 4.28: Velocity Contour around Savonius rotor Model 2 at $Re = 1.40 \times 10^5$.

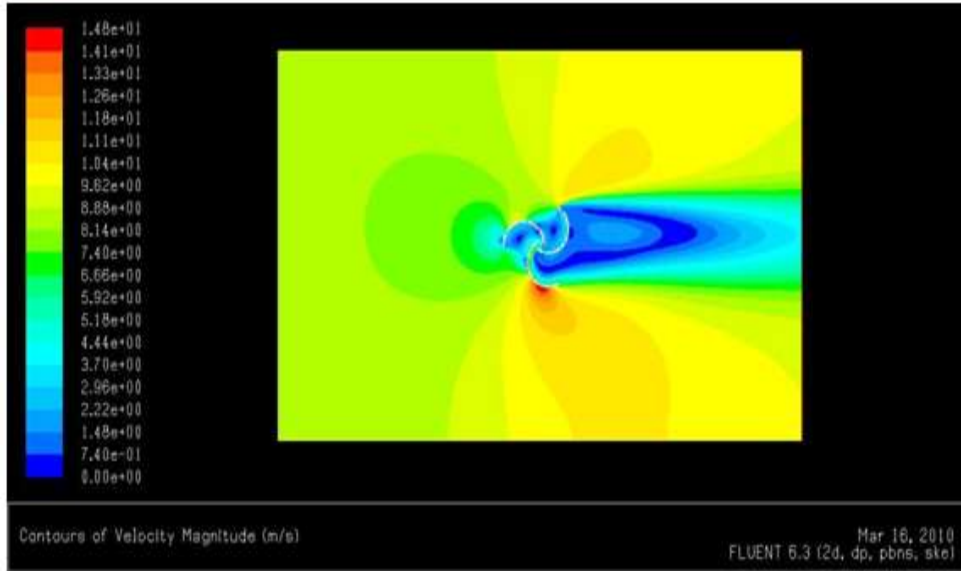


Figure 4.29: Velocity Contour around Savonius rotor Model 2 at $Re = 1.19 \times 10^5$.

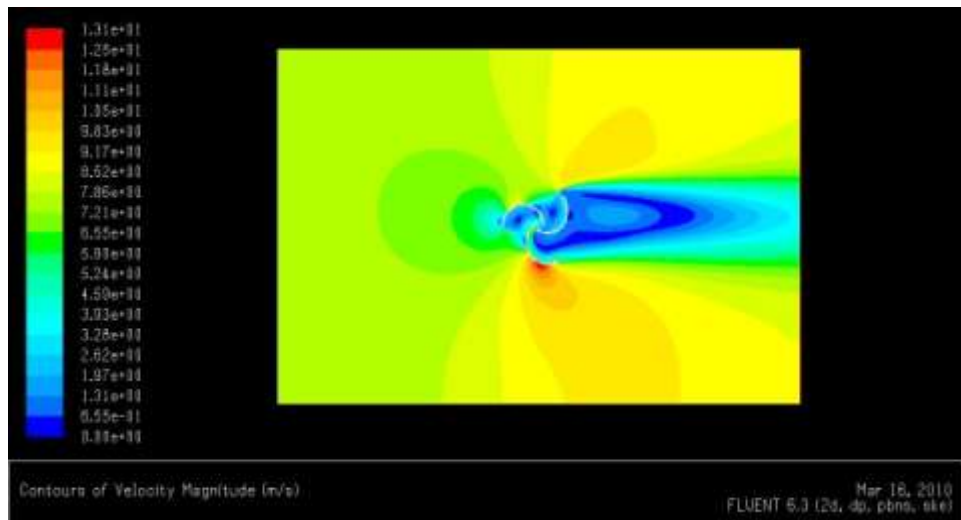


Figure 4.30: Velocity Contour around Savonius rotor Model 2 at $Re = 1.06 \times 10^5$.

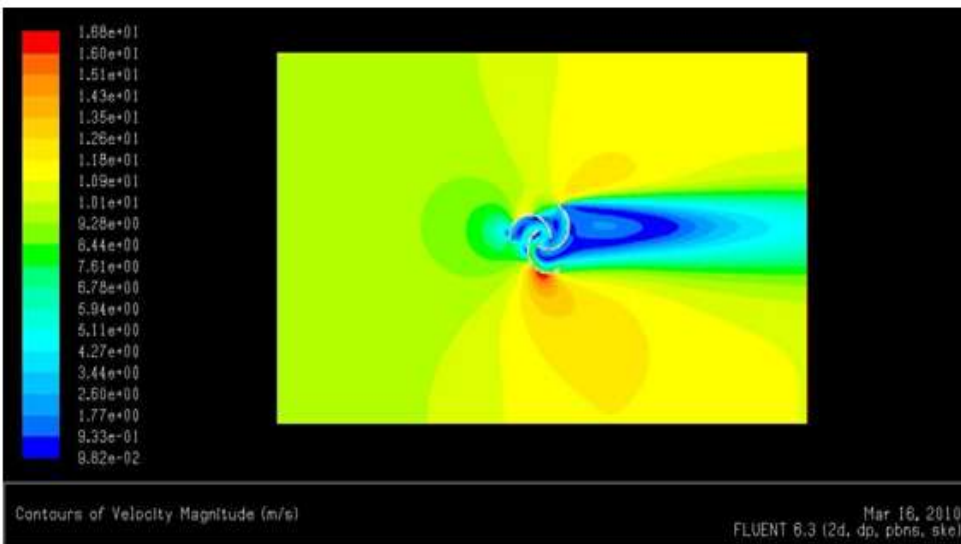


Figure 4.31: Velocity Contour around Savonius rotor Model 3 at $Re = 1.24 \times 10^5$.

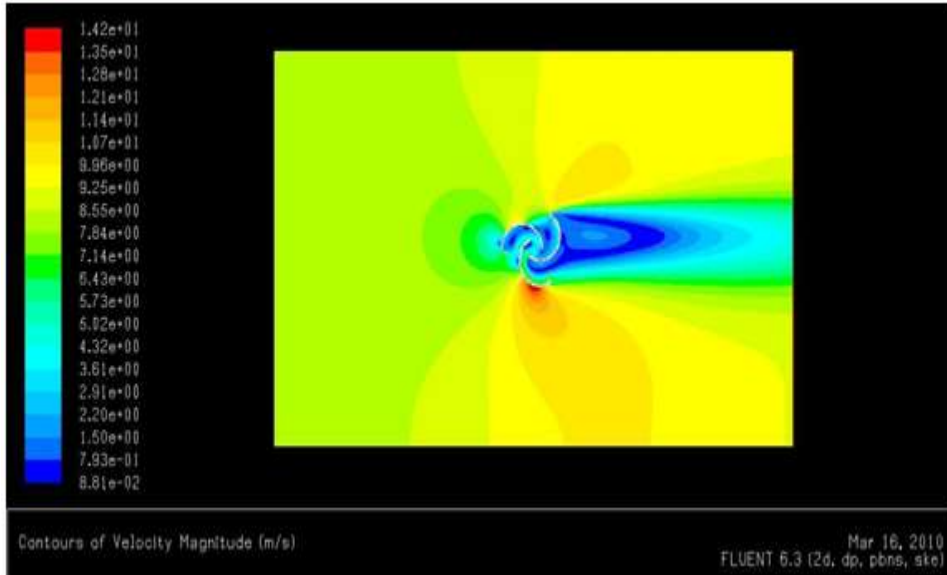


Figure 4.32: Velocity Contour around Savonius rotor Model 3 at $Re = 1.06 \times 10^5$.

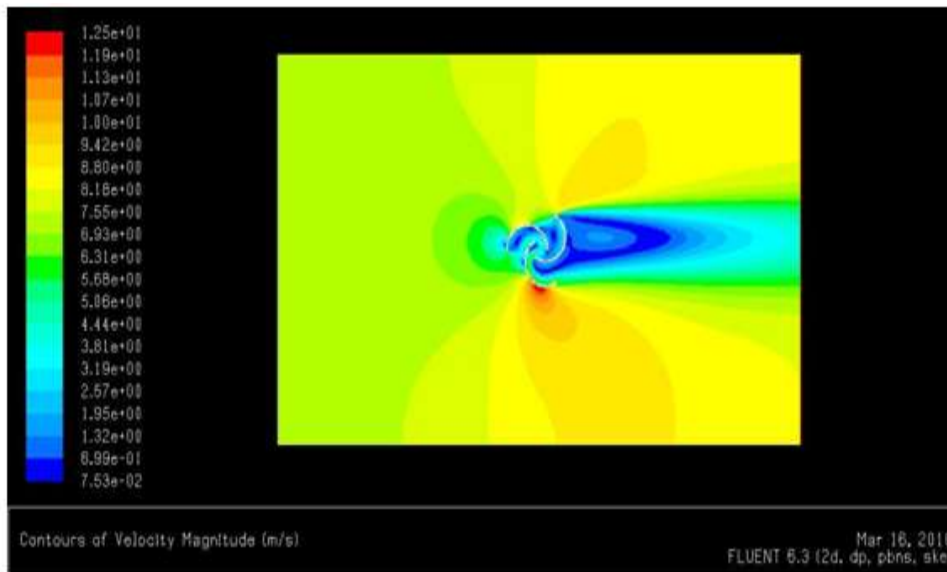


Figure 4.33: Velocity Contour around Savonius rotor Model 3 at $Re = 9.44 \times 10^4$.

IV. Conclusion

From this current study, analysis and results of this research work, the following conclusions can be made:

- i. For Model 1 with $Re = 1.22 \times 10^5$, Model 2 with $Re = 1.06 \times 10^5$, and Model 3 with $Re = 9.94 \times 10^4$ experimental torque coefficient (C_t) shows higher and positive values compared to other Reynolds numbers. It also shows that lower Reynolds number gave better torque coefficient (C_t) variation with the increase of the angle of rotation for each Model. Model 2 demonstrate better experimental torque coefficient (C_t) for all three different wind speeds (9.66 m/s, 8.23 m/s, and 7.33 m/s).
- ii. For Model 1 with $Re = 1.22 \times 10^5$, Model 2 with $Re = 1.19 \times 10^5$, and Model 3 with $Re = 9.94 \times 10^4$ experimental power coefficient (C_p) shows higher and positive values compared to other Reynolds numbers.

References

- [1]. Aldoss, T. K., Obeidat, K. M. (1987) Performance analysis of two Savonius rotors running side by side using the discrete vortex method, Wind Engineering, 11, 79-88.
- [2]. Altan, B. D., Atilgan, M. (2008). An experimental and numerical study on the improvement of the performance of savonius wind rotor. Energy conversion and management, 3425-3432.

- [3]. Atan, B. D., Atilgan, M, Ozdamar, A. (2008). An Experimental study on improvement of savonius rotor performance with retaining. Experimental thermal and fluid science, 32, 1673-1678
- [4]. enjanirat, S., Sankar, L., & Xu, G. (2003). Proceedings of 41st aerospace sciences meeting and exhibit Evaluation of turbulence models for the prediction of wind turbine aerodynamics. Reno, Nevada.
- [5]. Diaz, F., Gavalda, J., Massons, J. (1991) Drag and lift coefficients of the Savonius wind machine, Journal of Wind Engineering. 15, 240-246. Fluent 6.3 user guide
- [6]. Fujisawa, N. (1992). On torque mechanism of savonius rotors. Journal of Wind Engineering and Industrial Aerodynamics, 40, 227-292
- [7]. Fujisawa, N., Gotoh, F. (1994) Experimental study on the aerodynamic performance of a Savonius rotor, ASME Journal of solar energy engineering, 116, 148 – 152.
- [8]. Gupta, R., Biswas, A., Sharma, K. K. (2008). Comparative study of a three bucket savonius rotor with a combined three bucket savonius –three bladed darrieus rotor. Renewable Energy, 33, 1974-1981
- [9]. Hau, E. (2006) Wind turbines: Fundamentals, technologies, applications, economics. Germany. Springer- verlag berlin Heidelberg.
- [10]. Hayashi, T., Li, Y., Hara, Y., Suzuki (2004) Proceedings of European Wind Energy Conference and Exhibition, Wind tunnel test on a three stage out phase Savonius rotor, London, England.
- [11]. Hayashi, T., Li, Y., Hara, Y. (2005). Wind tunnel tests on a different phase three stage savonius rotor. JSME international journal, 48, 9-16.
- [12]. Islam, A. K. M. S., Islam, M. Q., Razzaque, M. M., & Ashraf, R., (1995), Static Torque and Drag Characteristics of an S-shaped Savonius Rotor and Prediction of Dynamic Characteristics, Wind Engineering, 19.
- [13]. Kamoji, M.A., Kedare, S.B., Prabhu, S.V. (2009). Performance test of helical savonius rotors. Renewable Energy, 34, 521-529
- [14]. Kamoji, M. A., Kedare, S. B. (2007) Proceedings of 5th AIAA International Energy Conversion Engineering Conference. Wind tunnel tests on a single stage helical Savonius rotor.
- [15]. Launder, B. E. and Spalding, D. B. (1972) Lectures in Mathematical Models of Turbulence. Academic Press.
- [16]. Lida, A., Kato, K. & Mizuno, A. (2007). Proceedings of 16th Australasian fluid mechanics conferences. Numerical simulation of unsteady flow and aerodynamic performance of vertical axis wind turbine with LES. Gold Coast, Australia.
- [17]. McWilliam, M., Johnson, D.A. (2008). Velocity measurement of flow around model vertical axis wind turbines. International Journal of Green Energy, 5, 55-68.
- [18]. Menet, J.L., Bourabaa, N. (2004). Proceedings of European Wind Energy Conference. Increase in the Savonius Rotor Efficiency via a Parametric Investigation. London, UK
- [19]. Menet, J.L., Valdes, L.C., Menart, B. (2001). A comparative calculation of the wind turbines capacities on a basis of the L- σ criterion, Renewable Energy, 22, 491-506.
- [20]. Newman, B. G. (1974). Proceedings of symposium on wind energy: achievements and potential. Measurements on a savonius rotor with a variable gap. Sherbrooke, Canada.
- [21]. Patankar, S. V., (1980) Numerical Heat Transfer and Fluid Flow, Hemisphere Publishing Corporation.
- [22]. Paraschivoiu, I. (2002). Wind turbine design: with emphasis on Darrieus concept. Montreal, Canada: Polytechnic International Press.
- [23]. Pike Research LLC (2009). Wind Energy Outlook for North America Wind Power Generation Capacity and Turbine Deployments:

Dr.M.S.Murthy "Computational Analysis Of Aerodynamic Characteristics With Different Overlap Ratio Using CFD "International Journal of Engineering Science Invention (IJESI), vol. 07, no. 09, 2018, pp 59-70